Interleaved Isophoric Sparse Arrays for the Radiation of Steerable and Switchable Beams in Satellite Communications

O.M. Bucci, *Fellow, IEEE,* S. Perna, *Senior Member, IEEE,* and D. Pinchera, *Senior Member, IEEE*

***Abstract*.- We address the synthesis of isophoric sparse ring arrays for full Earth coverage from GEO satellites by means of steerable beams, switchable between two different widths. In particular, we pursue the desired beam zooming/shrinking through two interleaved sparse arrays deployed over the available circular aperture. To this aim, we propose two different antenna architectures: in one case, the two beams are radiated by two separate interleaved arrays; in the other case, the two beams are instead radiated by two interleaved arrays that share a common part of their layouts. Both the proposed architectures allow us to exploit a synthesis procedure that calculates the two interleaved arrays separately, through the cascade of two steps, both implemented with a (computationally) very efficient deterministic density tapering approach. The proposed strategy allows to obtain isophoric sparse layouts satisfying the required design constraints with a significant reduction of the control points with respect to the solution achievable exploiting non-interleaved isophoric sparse arrays.**

***Index Terms*— Antenna arrays, Sparse array antennas, Antenna radiation pattern synthesis, Satellite antennas**

I. INTRODUCTION

Within the class of Direct Radiating Array (DRA) antennas, an increasing attention is today paid to the isophoric sparse ones, namely, non-periodic arrays employing equi-amplitude radiating elements [1]-[8].

However, their synthesis is not straightforward, and in practical cases it can be addressed only through smart approaches [6]-[21] aimed at finding sub-optimal solutions. With particular reference to satellite applications, the exploitation of some of these approaches [7], [8], [16]-[18] allowed us to find solutions capable of effectively fulfilling the requirements listed by the European Space Agency (ESA) through the Invitation To Tenders (ITTs) [3], [4]. In particular, in [8] we have addressed the synthesis of sparse ring arrays for full Earth coverage from GEO satellites by means of multiple beams, steerable up to about 8° and switchable between two widths (0.65° and 3.25°). More specifically, in [8] both the narrow and the wide beams are radiated by the same array and the required beam zooming/shrinking is achieved by means of a phase-only control. As shown in [8], the synthesis of such a kind of architecture involves a number of issues. First, since the array layout is strongly dependent on the width of the radiated beam, the synthesis strategy must tailor the whole array geometry *simultaneously* to both the desired beam-widths. This makes the exploitation of the quick deterministic approaches quite difficult [9], [11], [13], [16], [17], [20], relying on the *emulation* of an optimal continuous source satisfying the power pattern requirements. Indeed, the optimal reference source for the wide beam (3.25°) becomes *complex* when it is forced to have the same dimension of the optimal source for the narrow beam (0.65°). Thus, the deterministic approaches, which are tailored to *real* reference sources, should be extended to *complex* ones. However, this has rigorously been achieved up to now only for the 1D case [22]. For these reasons, in [8] we developed a hybrid approach, computationally less efficient than the deterministic ones. By doing so, we have synthesized an array satisfying the design specifications with a number of feeds 80% greater than that required to radiate (still with an isophoric sparse array) only the narrow steerable beam. This increase is also due to the fact that if we want to radiate both beams with the same array, the dimension of the feeds must be smaller than that required to radiate only the narrow beam.

In this work, with reference to the application scenario addressed in [8], in order to reduce the number of control points of the sparse array we propose to pursue the desired beam zooming/shrinking through two interleaved sparse arrays, one for each beam-width, deployed over the available circular aperture. To fulfill this aim, two novel architectures are presented: the first one consists of two separate arrays, whereas the second one consists of two arrays that share a common part of their layouts. Interestingly, the synthesis of these proposed architectures presents a number of advantages with respect to the antenna synthesis carried out in [8]. First, the optimal continuous reference sources for the wide and narrow beams can have different dimensions. This makes it possible to deal, for both beams, with *real* optimal sources, thus rendering the exploitation of quick deterministic approaches for the synthesis of the two interleaved layouts easier. Second, to radiate the wide and the narrow beam, respectively, we can use different feeds (actually, for the interleaved-shared architecture, this property holds only for

Ovidio Mario Bucci is with IREA-CNR, Napoli, Italy. E-mail: bucci@unina.it
Stefano Perna is with DI, Università degli Studi di Napoli "Parthenope", Napoli, Italy, and with IREA-CNR, Napoli, Italy. E-mail: perna@uniparthenope.it.
Daniele Pinchera is with DIEI, Università degli Studi di Cassino e del Lazio Meridionale, Cassino, Italy. E-mail: pinchera@unicas.it.
All the authors are also with CNIT, Parma, Italy.

the non common part of the arrays). This allows the number of control points of the whole array to be reduced by exploiting, at least for the narrow beam, feeds larger than those used in [8].

More generally, to achieve the two interleaved arrays we can move towards a synthesis strategy which differs completely from that in [8]. Indeed, in [8] the whole array geometry is synthesized by simultaneously enforcing the constraints imposed by both the desired beam-widths. Conversely, in this work, the two interleaved array layouts, one for each beam-width, are not obtained simultaneously, but through an easier synthesis scheme consisting of the cascade of two separate steps, one for each layout. For both steps, we exploit a synthesis procedure based on the Deterministic Approach (DA) presented in [16] and further developed in [17] to also carry out the feed size tapering and in [7] to allow the 8° beam steering ability needed to guarantee full Earth coverage.

The work is organized as follows. In Section II, we briefly recall the considered application scenario along with the corresponding antenna synthesis constraints. In Section III, to clarify the context of the presented architectures, we demonstrate that the two different required patterns can be radiated with two different arrays of two different sizes and enclosed in the available area. The proposed synthesis approaches are described in Section IV. Section V shows the achieved results. The conclusions are drawn in the last Section.

II. Statement of the Problem

We refer to the same application scenario addressed in [8] according to the ESA specifications listed in the ITT in [4]. More specifically, what is required is to achieve full Earth coverage from a GEO satellite by means of multiple steerable and zoomable beams (the reader is referred to [8] for more details). For this multi-spot scenario, the required constraints can be translated, for the boresight beam, into the following mask:

$$\begin{aligned} &D(\theta,\varphi) \geq D_{WC} && \text{for } \theta \leq \theta_{EOC} \\ &D(\theta,\varphi) \leq D_{WC} - 20\ dB && \text{for } \theta_{NIC} \leq \theta \leq \theta_{EOE} \end{aligned} \quad (1)$$

where

$$\theta_{EOC} \in \left\{ \frac{\mathrm{BW_n}}{2} , \frac{\mathrm{BW_w}}{2} \right\} = \{0.325° , 1.625°\} \quad (2)$$

$$\theta_{\mathrm{NIC}} \in \{\theta_{\mathrm{NICn}} , \theta_{\mathrm{NICw}}\} = \{0.795°, 3.975°\} \quad (3)$$

In eqs.(1)-(3), $D(\cdot)$ is the array directivity (expressed in dBi), being θ and φ the elevation and azimuth antenna angles, respectively. Moreover, the angle θ_{EOE} is the maximum inside Earth angle, θ_{EOC} is the angle marking the spot's Edge Of Coverage (EOC), while θ_{NIC} is the EOC angle of the nearest "iso-color" (that is, iso-frequency and iso-polarization) spot. Note that $\mathrm{BW_n}$ and $\mathrm{BW_w}$ in (2) are the required narrow and wide beam-widths, respectively, whereas θ_{NICn} and θ_{NICw} in (3) are the two values of θ_{NIC} required for the two different beam-widths. Finally, D_{WC} is the minimum directivity within the coverage. It is remarked that the maximum allowable Side Lobe Level (SLL), with respect to D_{WC}, is equal to -20 dB, see (1). Also, assuming that the array boresight direction points at the equator, we have that θ_{EOE} in (1) is about 8°.

Turning to the scanned beams, to guarantee Full Earth coverage, the constraints in (1)-(3) must be satisfied also when steering the boresight beam up to θ_{EOE}-θ_{EOC}.

Finally, all the aforementioned requirements must be fulfilled with an overall array diameter of less than 120 λ, λ being the carrier wavelength.

III. Preliminary Analysis

To synthesize the two interleaved isophoric arrays different strategies can be possible. In order to clarify the rationale behind the strategy that we propose, we address a preliminary analysis as follows.

First of all, we note that the two layouts tailored to the two different beam-widths required in (1)-(3) can have significantly different dimensions. To clarify this point to a greater extent, it is convenient to move towards *continuous* circular sources, rather than *discrete* ones. Indeed, the synthesis of the optimal (namely, guaranteeing the maximum D_{WC}) continuous circular source capable of radiating the boresight pattern satisfying the requirements in (1)-(3) can be easily carried out through the method proposed in [23]. This allows for a straightforward investigation of the impact of the aperture size on the antenna performances, for both the desired beam-widths.

The analysis relevant to the narrow beam has already been performed in [23], where it is shown that D_{WC} of the optimal continuous source rapidly increases up to aperture diameters of approximately 85 λ and remains almost constant for aperture diameters even larger than 120 λ. Accordingly, to radiate the narrow beam we need an aperture diameter as wide as (at least) 85 λ. Interestingly, for aperture diameters in our range of interest, the optimal continuous source turns out to be real.

Turning to the wide beam, we have carried out an analysis similar to that performed in [23] for the narrow beam. More specifically, we have applied the algorithm in [23] by considering different aperture dimensions and the boresight pattern constrains of the wide beam in (1)-(3). The results are reported in Fig.1. As can be seen, the optimal D_{WC} quickly increases up to aperture diameters of approximately 18-20 λ and then stays almost constant. Accordingly, there is little point in increasing the aperture diameter further. Interestingly, up to 27 λ, the optimal continuous source turns out to be real and positive. Further increase of the aperture size forces the optimal continuous source to remain real but to become negative at the edge of the aperture itself. For array diameters larger than about 35 λ, the optimal solution becomes complex and thus different from that provided by the algorithm in [23]. According both to the plot of Fig. 1 and to the analysis reported in [23], we can draw the conclusion that the size of the layout tailored to the wide beam can be significantly

This article has been accepted for publication in a future issue of this journal, but has not been fully edited. Content may change prior to final publication. Citation information: DOI 10.1109/TAP.2016.2647685, IEEE Transactions on Antennas and Propagation

smaller than that required to radiate the narrow beam. Therefore, the array layout that radiates the wide beam can be profitably located in the core part of the available aperture. This, in turns, suggests an easily implementable synthesis scheme, which calculates the two interleaved layouts through the cascade of two separate steps.

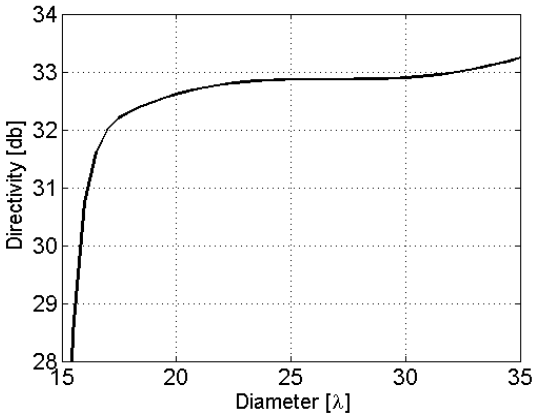

Fig. 1. Wide beam: directivity of the optimal continuous sources relevant to circular apertures of different diameters. The reported directivity is the minimum within the required beam coverage (D_{WC}).

The first step carries out the synthesis of the inner sparse layout tailored to the wide beam, without enforcing any geometrical constraint related to the presence of the other layout to be synthesized.

The second step performs the synthesis of the sparse layout tailored to the narrow beam by taking into account that some areas of the available aperture are already occupied by the feeds of the layout synthesized through the first step. ~~To~~ In this regard, for the design of the layout to be synthesized through this second step we propose two options, which lead to two different antenna architectures.

For the radiation of the narrow beam, the first possibility is to exploit only the circular crown not occupied by the inner array. Indeed, from the analysis shown in [7] we expect that giving up on the inner rings will have no impact on the level of the pseudo-grating lobes of the narrow-beam pattern. On the other hand, a reduction of its directivity is unavoidable.

To minimize such reduction, a different option could be adopted, namely to exploit the entire circular aperture for the narrow beam radiation, enforcing the constraint that the core of the array to be synthesized should coincide with the already synthesized layout tailored to the wide beam.

Both the proposed architectures are depicted in Fig. 2.

It is to be noted that the two-steps synthesis strategy described above to achieve the two architectures of Fig. 2 allows the two synthesis problems related to the two different required beam-widths to be addressed separately. This represents a key difference with respect to the synthesis strategy adopted in [8], where the isophoric sparse array capable of radiating the two different beams via a phase-only control is synthesized by simultaneously enforcing the constraints imposed by the two desired beam-widths. The implications related to this difference will be clarified in the next Section, which addresses the implementation of the proposed two-step synthesis scheme.

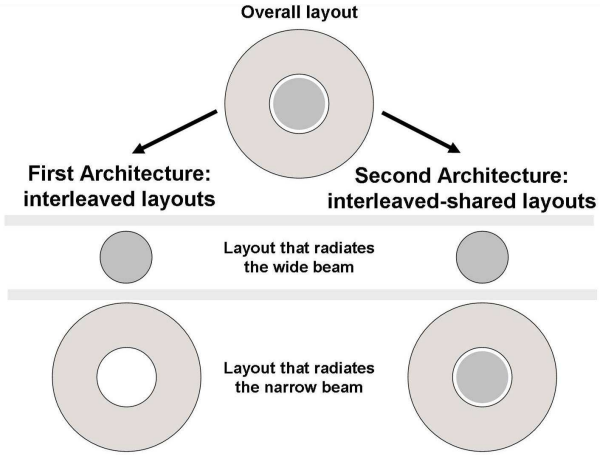

Fig. 2. The two proposed array architectures that pursue the desired beam zooming/shrinking through two interleaved sparse arrays, one for each beam-width. Left: the inner layout radiates the wide beam, whereas the outer one radiates the narrow beam. Right: the inner array radiates the wide beam; moreover, it represents the inner part of a larger array that radiates the narrow beam.

IV. Array Synthesis

This Section addresses the implementation of the two-steps synthesis approach discussed in Section III. More specifically, the implementation of the first step (which is described in Subsection *B*) is the same for both the proposed architectures depicted in Fig. 2. Conversely, the implementation of the second step depends on which architecture we intend to achieve; thus, the details on this synthesis step are presented in two different Subsections (*C* and *D*). Moreover, for both the steps and for both the proposed architectures, we exploit a (computationally) very efficient synthesis procedure based on the Deterministic Approach (DA) in [16], which is briefly recalled in the next Subsection (*A*).

A. Deterministic Approach (DA).

The Deterministic Approach (DA) originally presented in [16] exploits a given continuous real, azimuthally symmetric, reference source, say i(ρ) (being ρ the radial coordinate of a generic point on the available circular aperture) capable of fulfilling at the best the directivity constraints required for the boresight spot of the array.

Once i(ρ) is calculated, the DA subdivides the available aperture into a number of adjacent concentric rings, and each of them into equal sectors, all subtending the same volume of i(ρ). Subsequently, the DA properly locates one array element for each computed iso-volume sector. To compute the iso-volume that each sector must subtend, it is necessary to fix *a-priori* the core geometry of the array, namely, the geometry of the most internal ring (or of the most internal rings). Also, the shape of all the considered iso-volume sectors must be chosen in such a way as to fulfill the geometrical constraints imposed

This article has been accepted for publication in a future issue of this journal, but has not been fully edited. Content may change prior to final publication. Citation information: DOI 10.1109/TAP.2016.2647685, IEEE Transactions on Antennas and Propagation

on one hand by the shape of the employed feeds [16], [17] and on the other by the maximum steering angle required for the radiated beam [7].

Summing up, the DA in [7], [16], [17] calculates the sparse array layout starting from the following inputs: the external reference source i(ρ), the core geometry of the array, the geometric characteristics of the array elements, the maximum allowable azimuth inter-element distance.

B. Synthesis of the layout tailored to the wide beam.

The first step of the proposed procedure calculates the inner layout tailored to the wide beam without enforcing any geometrical constraint related to the presence of the other layout to be synthesized.

To this regard, the preliminary analysis carried out in Section III has shown that to radiate the wide beam, an aperture diameter of approximately 18-20 λ is appropriate; moreover, for such an aperture dimension, the corresponding optimal continuous source is real and positive. Accordingly, to achieve the inner layout we can straightforwardly apply the original DA recalled in Subsection IV *A*.

C. Synthesis of the layout tailored to the narrow beam: interleaved architecture.

For the first architecture of Fig. 2 (consisting of two interleaved, separate, layouts), the second step has to enforce the constraint that only the circular crown, not occupied by the inner array, can be exploited to synthesize the array tailored to the narrow beam.

To find the most appropriate synthesis strategy for the implementation of this step, it is convenient, as usual, to first investigate the optimal continuous source relevant to the available circular crown. To this aim, we can still exploit the approach in [23] for the circular apertures, by carrying out just a slight modification aimed at accounting for the changed aperture geometry, which in this case is a circular crown. In particular, with respect to the procedure shown in [23] for the synthesis of the optimal continuous source $i(\rho)$ defined over a circular aperture, we just have to add the constraint that $i(\rho)=0$ for $\rho \in [0, Ri]$, Ri being the radius of the circular aperture already occupied by the inner array. Since this additional constraint is linear, the whole problem remains convex as the one considered in [23]. In this way, enforcing the boresight pattern constrains of the narrow beam in (1)-(3), we have investigated the performances of the optimal continuous sources relevant to circular crowns of different sizes. More specifically, according to the analysis of Section III, we have considered an inner diameter of 20 λ, and different external diameters (always less than the threshold of 120 λ imposed by the system requirements, see Section II). By doing so, we have managed to obtain a real and positive optimal continuous source in all the range of our interest, enabling us to once more straightforwardly exploit the DA recalled in Subsection IV *A*. The directivity results relevant to the calculated optimal continuous sources are reported in Fig. 3 (continuous line). Similarly to what has been observed in Section III for the circular aperture, we also note that for the circular crown the D_{WC} quickly increases up to a certain threshold of the external diameter to then become almost constant. In particular, for Ri=20 λ this threshold is about 95 λ. Obviously, different

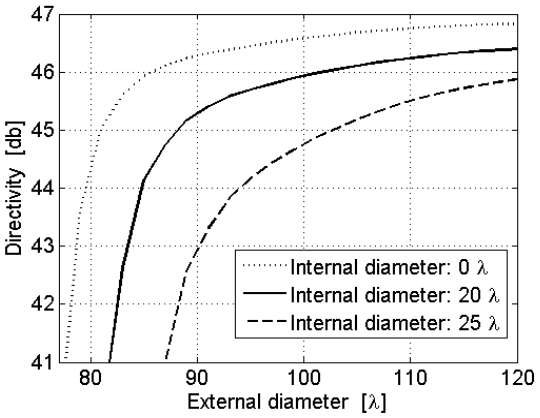

Fig. 3. Narrow beam: directivity of the optimal continuous sources relevant to circular crowns enclosed by different internal and external radii. The reported directivity is the minimum within the required beam coverage (D_{WC}).

values of Ri lead to different thresholds. To show this, in Fig. 3 we also report the directivity results of the optimal continuous sources relevant to the circular crowns of internal radius Ri=25 λ (dashed line) and Ri=0 (dotted line). Of course, the latter curve corresponds to that obtained in [23] for the circular aperture case. It can be seen that the larger the internal circle of the crown the larger the value for the threshold after which the directivity becomes almost constant. From Fig. 3 we can also quantify the directivity loss of the optimal continuous source due to the aperture efficiency reduction related to the presence of the inner hole. Accordingly, when passing to the *sampled* solutions, namely the sparse arrays, we expect that giving up on the inner part of the available aperture will involve an unavoidable reduction of the narrow-beam directivity with respect to the solutions found in [7], [8]. To this regard, we stress that increasing the area devoted to the inner array over a certain threshold, impairs the directivity of the narrow beam but, according to the analysis performed in Section III, it does not increase the directivity of the wide beam. Therefore, at least for this architecture, it is convenient to keep the dimension of the inner layout as small as possible, that is, its diameter should be in the order of 18-20 λ.

Summing up, for the first architecture of Fig. 2, the second step can be based again on the DA recalled in Section IV *A*. To this regard, the plots of Fig. 3 provide useful guidelines for setting the external diameter of the layout to be synthesized.

Two final considerations are in order. First, as recalled above, this second step requires as input the radius Ri of the inner layout synthesized through the first step. We stress that this radius is typically smaller than that of the corresponding continuous aperture exploited during the first step, due to the radial density tapering applied by the DA. Thus, this information is available only after the first step is concluded. Second, as depicted in Fig. 4, which shows the overall adopted

This article has been accepted for publication in a future issue of this journal, but has not been fully edited. Content may change prior to final publication. Citation information: DOI 10.1109/TAP.2016.2647685, IEEE Transactions on Antennas and Propagation

synthesis scheme, all the inputs of the second step (except for the radius of the inner layout, as highlighted above) are independent of the first step. Accordingly, the size of the elements of the outer array can be set independently of the element size adopted for the inner layout. This allows for the circumvention of a drawback which arose in [8] where, due to the necessity to radiate both the narrow and the wide beam with the same layout, the size of the array elements turned out to be smaller than that found in [7] where only the narrow beam was radiated. Conversely, in our case, we can exploit, at least for the outer layout tailored to the narrow-beam, elements larger than those used in [8], with a corresponding reduction of the number of control points of the overall array.

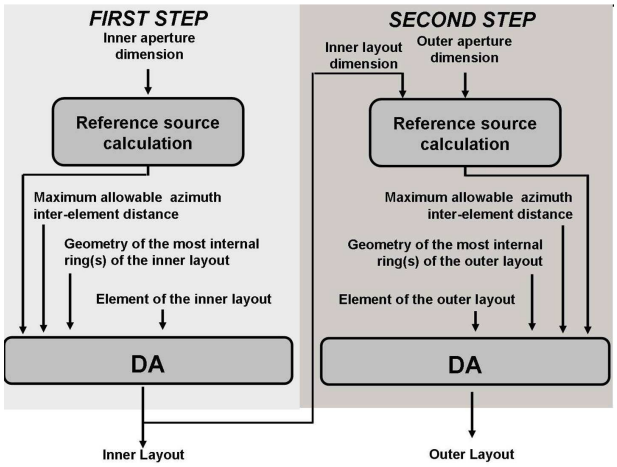

Fig. 4. Synthesis scheme for the design of the first architecture of Fig. 2 (interleaved layouts).

D. Synthesis of the layout tailored to the narrow beam: interleaved-shared architecture.

To achieve the second architecture of Fig. 2 (interleaved-shared layouts), the second step has to enforce the constraint that the core geometry of the array to be synthesized must coincide with the inner layout synthesized through the first step. This kind of constraint makes the second step very easy to implement, again by exploiting the DA recalled in Section IV *A*.

More specifically, we start from the optimal continuous source tailored to the narrow-beam and relevant to the entire available circular aperture (of radius *Ro*), also including the area (namely, a circular aperture of radius *Ri*) occupied by the inner layout synthesized through the first step. Once the optimal source $i(\rho)$ is calculated, the DA can be applied by focusing on the following issues.

According to the main rationale of the DA, starting from the core geometry of the array to be synthesized, we have to subdivide the remaining area in equi-volume sectors. Interestingly, in our case the core geometry of the array to be synthesized is represented by the layout already synthesized through the first step and tailored to the wide beam. This implies first of all that the area to be subdivided in equi-volume sectors is represented by the circular crown not occupied by the inner array. Moreover, to compute the iso-volume that each sector of this area must subtend, we have to exploit on the one hand the inner layout tailored to the wide beam, and on the other the continuous reference source $i(\rho)$ tailored to the narrow-beam. More specifically, let us denote with *Ni* the number of elements of the inner layout tailored to the wide beam, and with I_i the volume of $i(\rho)$ subtended by the circle of radius *Ri*. The iso-volume that each sector of the available circular crown (enclosed by the radii *Ri* and *Ro*) must subtend is given by [17]:

$$vol = \alpha \frac{Ii}{Ni} \tag{4}$$

where the coefficient α accounts for the possibility that the array element to be used in the outer layout may be different from that exploited in the inner layout. More specifically, α is the ratio between the (copolar) patterns (sampled in the direction of maximum radiation) of the element of the outer and the inner layouts [17]. In particular, if we exploit for the outer layout the same element used for the inner one, we have to set α=1. More generally, similarly to the architecture analyzed in the previous Subsection, for this interleaved-shared architecture we can also exploit for the outer layout elements larger than those used in [8], with a corresponding reduction of the number of control points of the overall array. It is worth stressing that by doing so we obtain that the overall layout tailored to the narrow beam exploits elements of two different sizes. Therefore, unlike the architecture analyzed in Subsection IV*C*, in this interleaved-shared architecture the layout tailored to the narrow beam also exploits, in addition to the standard element-density tapering strategy, the more advanced element-size tapering one [17], [18], [20], [24].

Summing up, to achieve the second architecture of Fig. 2, the second step is based again on the DA recalled in Section IV *A*. More specifically, as depicted in Fig. 5, which shows the overall adopted synthesis scheme, this step initially calculates the continuous reference source tailored to the narrow beam and relevant to the entire available circular aperture. In this

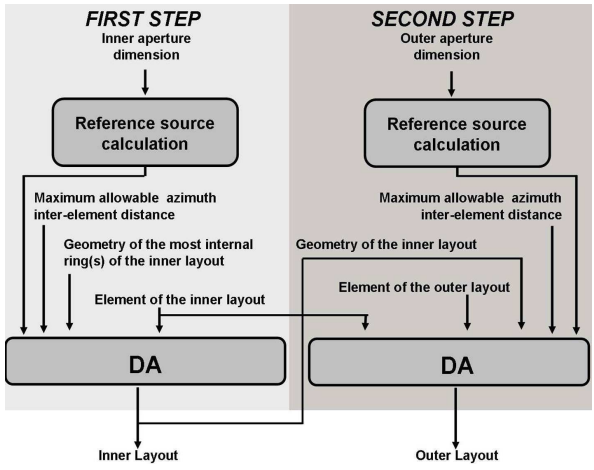

Fig. 5. Synthesis scheme for the design of the second architecture of Fig. 2 (interleaved-shared layouts).

case this operation is independent of the results obtained

This article has been accepted for publication in a future issue of this journal, but has not been fully edited. Content may change prior to final publication. Citation information: DOI 10.1109/TAP.2016.2647685, IEEE Transactions on Antennas and Propagation

through the first step. Once the continuous source is calculated, the second step carries out the DA by exploiting the radius *Ri* as input from the first step, the number *Ni* and the e.m. features of the
elements of the inner layout.

V. RESULTS

The effectiveness of the proposed architectures is assessed in the following.

The array elements considered hereafter are circular feeds optimally synthesized as shown in [7] to maximize the array directivity within the entire area covered by the transmitted steerable beam. Moreover, in order to fulfill the requirement of full Earth coverage from GEO orbits, the inter-element azimuth distance between the radiating feeds has been forced to be smaller than 3.2 λ [7].

Let us start from the layout tailored to the wide beam.

Along the lines of Section III, we have synthesized the optimal continuous reference source defined over a circular aperture of 20 λ diameter and fulfilling the requirements (1)-(3) for the boresight wide-beam. More specifically, we have enforced a maximum SLL (with respect to the minimum directivity within the beam) of -23 dB, which is 3 dB tighter than that required by the array specifications, see (1). As better discussed later on (when the layouts tailored to the narrow beam are shown), this choice is aimed at accounting for the SLL impairment induced by the shape of the element pattern when steering the array boresight beam [7]. Following the reference source calculation, subsequent application of the processing steps highlighted in the left part of Figs. 4 and 5 has led to the 43-element layout reported in Fig. 6. The diameter of the used circular feeds is equal to 1.9 λ. The right panels of Fig. 6 show also the superposition of the corresponding array directivity φ-cuts for the boresight (top) and the maximally scanned beam (bottom). The corresponding main array characteristics are reported in Table I, while the detailed ones are listed in Table II. It is noted that the radiated wide beam fulfills the requirements (1)-(3), apart from the SLL of the maximally scanned beam, which is higher than the required one for a very marginal amount (less than 0.1 dB), due to a pattern contribution well localized around θ=-5°. For comparison, Table I reports also the results relevant to an optimal non-isophoric, fully populated, ring array layout employing the circular 1.9 λ feeds over the same circular aperture covered by the sparse array of Fig. 6. Such a layout, which employs 82 elements, has been synthesized by extending to the discrete case the method devised in [23] for the continuous source. It is stressed that the overall directivity of the non-isophoric array turned out to be (for both the boresight and the maximally scanned beam) about 2 dB higher than that of the isophoric one, which however employs almost half of the elements. This means that the increase of the number of elements of the fully populated (non-isophoric) array is associated with an increase of the directivity lower than that expected from the increase of the filled area. To better clarify this point, we can focus, as in [7], on the directivity per control point, say $\eta=D_{WC}-10\log_{10}N$, N being the overall number of elements. Observing Table I it can be noted that the parameter η of the 43-element isophoric array of Fig. 6 is better than that of the 82-element fully populated (non-isophoric) array. It is finally stressed that the 43-element isophoric array of Fig. 6 exploits 93.6% and 94.3% fewer elements, respectively, than the two isophoric arrays obtained in [8] to radiate the same beam. Notwithstanding, the directivity of the 43-element layout of Fig. 6 is just 1.3 and 1.8 dB lower than that achieved with the two layouts in [8]. As a consequence, the 43-element layout of Fig. 6 enables us to obtain a directivity per control point significantly higher (more than 10 dB) than that achieved with the two layouts in [8].

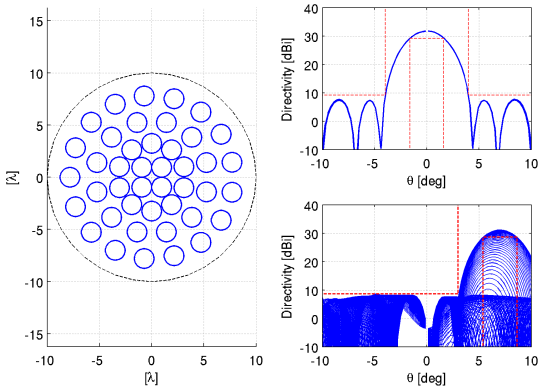

Fig. 6. Left panel shows the 43-element layout tailored to the wide beam case. Right panels show the superposition of the array directivity φ-cuts for the boresight (top) and the maximally scanned (bottom) beams. The employed circular feeds (of 1.9 λ diameter) have been optimally synthesized as shown in [7]

TABLE I
MAIN CHARACTERISTICS OF THE OBTAINED ZOOMABLE LAYOUTS

	Layout	Feed size	number of elements	DWC [dB]	SLL [dB]	η [dB]
Wide Beam Layout	Sparse (isophoric) Figure 6	1.9 λ	43	29.2 28.6	-21.5 -19.9	12.9
	Fully populated (not isophoric)	1.9 λ	82	31.3 30.6	-20.9 -20.1	12.1
Narrow Beam Layout Interleaved architecture	Sparse (isophoric) Figure 10	2.5 λ	460	41.3 40.1	-20.3 -19.9	14.7
	Fully populated (not isophoric)	2.5 λ	1076	44.6 43.3	-20.4 -20.0	14.3
	Sparse (isophoric) Figure 11	2.5 λ	628	41.8 40.6	-20.6 -20.3	13.8
	Fully populated (not isophoric)	2.5 λ	1461	45.2 43.9	-20.6 -20.2	13.6
Narrow Beam Layout Interleaved-shared architecture	Sparse (isophoric) Figure 14	1.9 λ 2.5 λ	43+ 381	41.6 40.4	-21.7 -20.2	15.4
	Fully populated (not isophoric)	1.9 λ 2.5 λ	82+ 1122	44.8 44.0	-20.7 -20.1	14.0

The SLL is calculated with respect to the minimum directivity D_{WC} within the beam.
D_{WC} and SLL values are relevant to the boresight (black) and the maximally scanned (red) beam

To this regard, it is remarked that the enormously higher

This article has been accepted for publication in a future issue of this journal, but has not been fully edited. Content may change prior to final publication. Citation information: DOI 10.1109/TAP.2016.2647685, IEEE Transactions on Antennas and Propagation

number of elements of the layouts obtained in [8] is due to the necessity to also radiate the narrow beam with the same layout: thus, the array sizes in [8] (about 90 λ) are significantly larger than those in the layout of Fig. 6.

Turning to the layout tailored to the narrow beam, we have carried out a massive parametric investigation by synthesizing several different arrays, exploiting different reference sources and setting different inter-element distances and element dimensions. This kind of analysis has been possible due to the very high computational efficiency of the exploited deterministic approach.

Let us start from the first architecture of Fig. 2 (interleaved layouts).

Along the lines of Section IV *C*, we have synthesized several continuous reference sources. In particular, we have considered circular crowns characterized by external diameters ranging from 105 λ to 130 λ. In all the cases, we have set an internal diameter equal to 17.6 λ, which is the external diameter of the 43-element core array reported in Fig. 6. Finally, for each considered circular crown we have synthesized different reference sources by enforcing different values (ranging from -23 dB to -20 dB) for the maximum allowable SLL of the radiated boresight beam. Starting from the synthesized continuous sources, a subsequent application of the processing steps highlighted in the right part of Fig. 4 has been performed setting different element dimensions (ranging from 2.5 λ to 3.2 λ) and inter-element distances. We have selected the most promising sparse arrays from those obtained, that is, the layouts which reach, for the maximally scanned beam, a SLL less than -19 dB. Corresponding results are shown in Figs. 7 and 8. In particular, Fig. 7 shows, for the boresight and the maximally scanned beam of the synthesized arrays, the SLL as a function of the overall number of employed elements. As is evident, in the plots we have exploited different symbols/colors, depending on the SLL constraint enforced during the synthesis of the continuous reference source. From Fig. 7 it is evident that to fulfill the -20 dB SLL array specifications also with the maximally scanned beam it is sufficient to enforce, for the boresight beam radiated by the continuous source, a SLL requirement 1 or 2 dB tighter. Turning to the achieved directivity, Fig. 8 shows, for the boresight and the maximally scanned beam of the synthesized arrays, the minimum directivity D_{WC} within the beam as a function of the overall number of employed elements. In this case, in the plots we have exploited different symbols/colors, depending on the number of rings of the synthesized arrays. As expected, from Fig. 8 we understand that, for a fixed number of rings, the higher the number of elements, the higher the corresponding array directivity. Interestingly, the plots also show that for a fixed number of elements, higher directivity is generally achieved with a smaller number of rings. Conversely, however, the number of rings does not appear to be directly related to the array performances in terms of SLL. This could be shown by reporting the same quantities of Fig. 7 while exploiting different symbols/colors as in Fig. 8, that is, depending on the number of rings of the synthesized arrays. However, for the sake of brevity, the so built plot is not reported here.

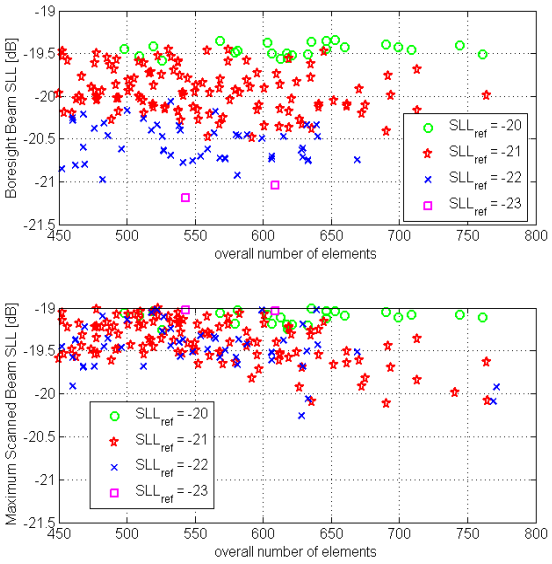

Fig. 7. Relevant to the radiation of the narrow beam through the first architecture of Fig. 2 (interleaved layouts).
SLL performances of the different arrays synthesized by exploiting different reference sources and setting different inter-element distances and element dimensions. Top and bottom panels show, for the boresight and the maximally scanned beam, respectively, the obtained SLL as a function of the number of employed elements. The SLL is calculated with respect to the minimum directivity within the beam (D_{WC}). Different symbols/colors are used in the plots, depending on the SLL constraint enforced during the synthesis of the continuous reference source.

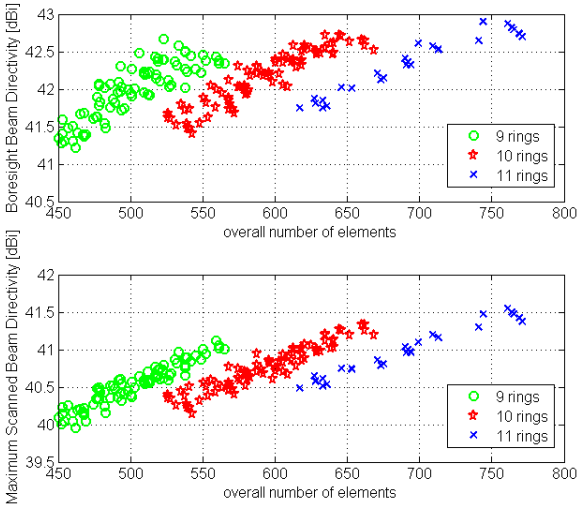

Fig. 8. Relevant to the radiation of the narrow beam through the first architecture of Fig. 2 (interleaved layouts).
Directivity performances of the different arrays considered in Fig. 7. Top and bottom panels show, for the boresight and the maximally scanned beam, respectively, the obtained minimum directivity within the beam (D_{WC}) as a function of the number of employed elements. Different symbols/colors are used in the plots, depending on the number of rings of the synthesized arrays.

From the plots of Fig.7 it is evident that to fully fulfill the

This article has been accepted for publication in a future issue of this journal, but has not been fully edited. Content may change prior to final publication. Citation information: DOI 10.1109/TAP.2016.2647685, IEEE Transactions on Antennas and Propagation

array specifications in (1)-(3) we have to employ a number of elements as large as 628. However, if we accept, at least for the maximally scanned beam, a SLL slightly higher than -20 dB, we can reduce to 460 the number of employed elements. In particular, the 460-element and 628-element layouts, picked up from the plots of Figs. 7, are shown in Figs. 9 and 10, respectively, along with the superposition of the corresponding array directivity φ-cuts for the boresight and the maximally scanned beams. In both cases the diameter of the used circular feeds is equal to 2.5 λ. Again, the corresponding main array characteristics are listed in Table I, while the detailed ones are reported in Table II. It is noted that the narrow beam radiated by the 460-element layout does not fulfill the -20 dB SLL requirement of the maximally scanned beam for a very marginal amount (less than 0.1 dB), due to a pattern contribution well localized around θ=-5°. Accordingly, such a layout certainly represents a good solution for our application. It is interesting to note that, compared to the 460-element layout of Fig. 9, the 628-element one of Fig. 10 allows the directivity to be improved by only 0.5 dB, with a corresponding decrease of the directivity per control point η (see again Table I).

We now discuss the comparisons with the non-isophoric, fully populated, ring array layouts defined over the same circular crowns covered by the sparse layouts of Figs. 9 and 10, respectively. Table I reports the main characteristics of such two fully populated ring arrays, both employing the same circular 2.5 λ feeds of the sparse layouts. These periodic arrays exploit 1076 and 1461 elements, respectively. By referring, for the sake of simplicity, only to the boresight beam, it can be seen that the overall directivities of the fully-populated (non-isophoric) arrays are about 3.3 dB and 3.4 dB higher than those of the corresponding isophoric ones of Figs. 9 and 10, respectively, which however exploit 57% fewer elements. As a consequence, both the synthesized sparse arrays show a much higher directivity per control point than that of the corresponding fully populated (non-isophoric) arrays, see again Table I.

We now illustrate comparisons with the sparse arrays obtained in [8]. The performances of the 628-element layout of Fig. 10, in terms of narrow beam SLL, are comparable to those of the 758-element layout synthesized in [8] to radiate the same beam: in both cases the SLL constraint is fully satisfied, even for the maximally scanned beam. Accordingly, we have obtained the same SLL performances achieved in [8] by exploiting 12% fewer elements. In this case, the narrow beam directivity D_{WC} of the 628-element layout of Fig. 10 is 0.9 dB lower than that of the 758-element–array directivity D_{WC} achieved in [8]: this leads to a very marginal impairment (0.1 dB) of the directivity per control point η. More interestingly, the performances of the 460-element layout of Fig. 9, in terms of narrow beam SLL, are quite similar to those of the 667-element layout synthesized in [8] to radiate the same beam: in both cases the SLL constraint on the most scanned beam is not satisfied for a very marginal amount. Accordingly, with the 460-element layout of Fig. 9 we have obtained the same SLL performances achieved in [8], by exploiting 31% fewer elements. Also, the narrow beam directivity D_{WC} of the 460-element layout of Fig. 9 is just 1.1 dB lower than that of the 667-element array directivity D_{WC} achieved in [8]: this leads to a 0.5 dB improvement of the directivity per control point η. To perform a fair comparison with the zoomable solutions achieved in [8], we now consider the overall zoomable architecture obtained by interleaving the 43-element layout of Fig. 6 and the layouts synthesized to radiate the narrow beam. More specifically, interleaving the 43-element and the 628-element layouts of Figs. 6 and 10, respectively, leads to a 671-element zoomable layout, which exploits 11% fewer elements than the 758-element layout synthesized in [8] with comparable SLL performances for both the wide and the narrow beam. On the other side, interleaving the 43-element and the 460-element layouts of Figs. 6 and 9, respectively, leads to a 503-element zoomable

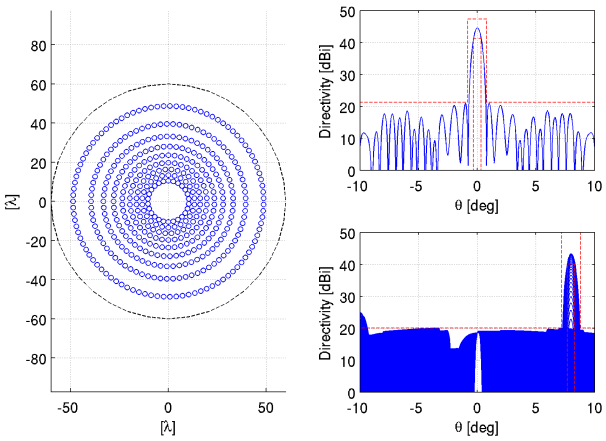

Fig. 9. Relevant to the radiation of the narrow beam through the first architecture of Fig. 2 (interleaved layouts). Left panel shows the 460-element layout tailored to the narrow beam case. Right panels show the superposition of the array directivity φ-cuts for the boresight (top) and the maximally scanned (bottom) beams. The employed circular feeds (of 2.5 λ diameter) have been optimally synthesized as shown in [7].

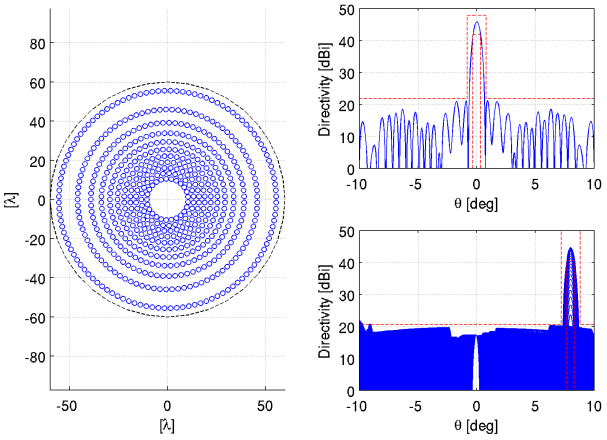

Fig. 10. Like Fig. 9, except for the number of elements exploited (628).

layout, which exploits 25% fewer elements than the 667-

This article has been accepted for publication in a future issue of this journal, but has not been fully edited. Content may change prior to final publication. Citation information: DOI 10.1109/TAP.2016.2647685, IEEE Transactions on Antennas and Propagation

element layout synthesized in [8] with comparable SLL performances for both the wide and the narrow beam. Accordingly, pursuing the required beam zooming/shrinking through the first architecture of Fig. 2 allows us to obtain, with a reduced number of elements, overall SLL performances comparable to those of the architecture proposed in [8], where the required beam zooming/shrinking is achieved by means of a phase-only control applied to a unique layout.

It is also to be noted that the 503-element and the 671-element layouts obtained here exploit a number of feeds 82% and 37%, respectively, greater than that of the 368-element layout found in [7] to radiate (still with an isophoric sparse array) only the narrow steerable beam.

Let us now turn to the second architecture of Fig. 2 (interleaved-shared layouts), discussed in Section IV *D*. In this case, we have considered circular apertures with external diameters ranging from 85 λ to 115 λ. Moreover, for each considered circular aperture we have synthesized different reference sources by enforcing different values (ranging from -25 dB to -21 dB) for the maximum allowable SLL. In this case, due to the increased size of the available apertures, which now include also the internal hole occupied by the layout tailored to the wide beam, it has been possible, for each fixed external diameter, to enforce SLL constraints even tighter than those considered above to synthesize the continuous sources exploited to obtain the layouts reported in Fig. 7.

Once the continuous sources have been synthesized, a subsequent application of the processing steps highlighted in the right part of Fig. 5 has been performed setting different element dimensions (ranging from 2.5 λ to 3.2 λ) and inter-element distances. As above, also in this case we have selected from the obtained sparse arrays those reaching, for the maximally scanned beam, a SLL less than -19 dB. Corresponding results are shown in Figs. 11 and 12, which are the counterparts of Figs. 7 and 8 for the interleaved-shared architecture of Fig. 2. The reported plots confirm the indications, which are not repeated here for the sake of brevity, provided by Figs. 7 and 8. We just remark that in Fig. 12 the overall number of rings of the synthesized arrays also includes the 4 rings of the core layout of Fig. 6.

From the plots of Fig. 11 we understand that to fully fulfill the array specifications in (1)-(3) (even for the maximally scanned beam) we can employ just 424 elements. Such a 424-element layout is shown in Fig. 13 along with the superposition of the corresponding array directivity φ-cuts for the boresight and the maximally scanned beams. Again, the corresponding main array characteristics are reported in Table I, while the detailed ones are listed in Table II. It is remarked once again that in this case the 424-element layout tailored to the narrow beam is obtained by sharing the 43-element layout of Fig. 6 and the 381-element layout synthesized through the second processing step highlighted in the right part of Fig. 5. Note that the outer layout employs circular feeds of 2.5 λ diameter, whereas the inner one employs circular feeds of 1.9 λ diameter. Accordingly, the overall layout depicted in Fig. 13 and tailored to the narrow beam exploits an element-size tapering [17], [18], [20], [24] in addition to the element-density one. As usual, Table I reports the comparison with the non-isophoric, fully populated, ring array layout deployed

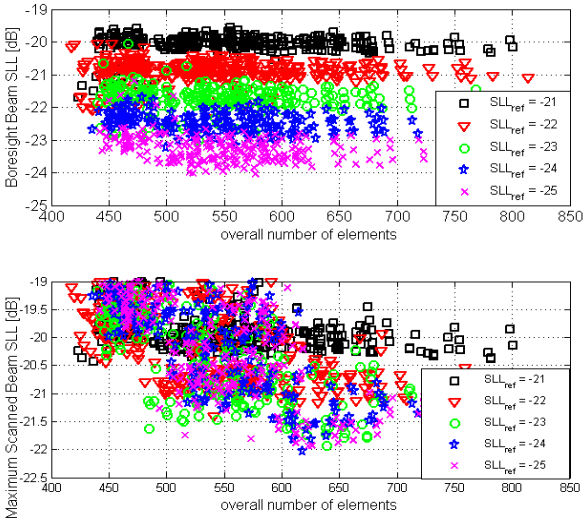

Fig. 11. Like Figure 7 except for the architecture considered, which in this case is the second of Figure 2 (interleaved-shared layouts).

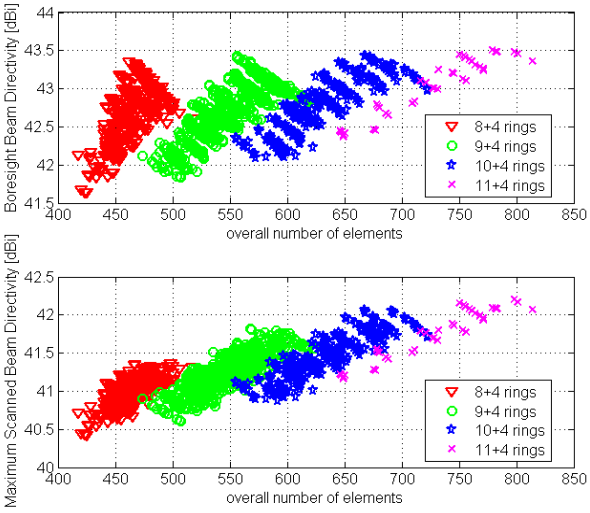

Fig. 12. Like Figure 8 except for the architecture considered, which in this case is the second of Figure 2 (interleaved-shared layouts).

over the same aperture of the 424-element layout of Fig. 13. To provide a fair comparison, for the fully populated layout we have applied the same element size tapering exploited in the sparse layout of Fig. 13. In particular, we have considered 1.9 λ diameter feeds within the circular aperture occupied by the core layout of Fig. 6, and 2.5 λ diameter feeds in the remaining area. It can be seen that the overall (boresight) directivity of the fully-populated (non- isophoric) array turned out to be about 3.2 dB higher than that of the corresponding isophoric one, which however employs 65% fewer elements.

This article has been accepted for publication in a future issue of this journal, but has not been fully edited. Content may change prior to final publication. Citation information: DOI 10.1109/TAP.2016.2647685, IEEE Transactions on Antennas and Propagation

Again, the sparse array shows a much higher directivity per control point compared to the fully populated (non-isophoric) array, see again Table I.

Comparisons between the interleaved-shared architecture of Fig. 13 and the interleaved architectures shown above are now provided.

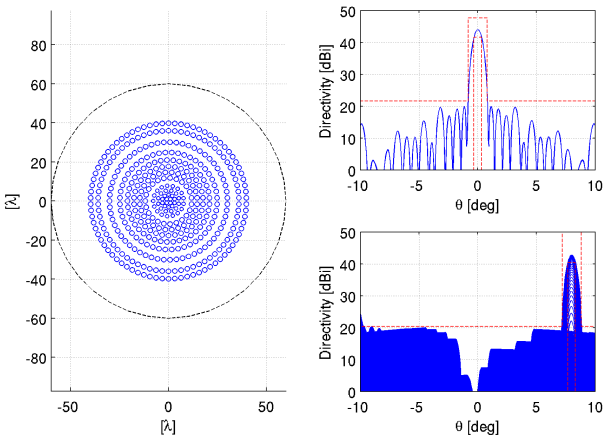

Fig. 13. Relevant to the radiation of the narrow beam through the second architecture of Fig. 2 (interleaved-shared layouts). Left panel shows the 424-element layout tailored to the narrow beam case. The core part of the array (namely, the first four rings) is coincident with the layout of Fig. 6. The diameter of the elements of the first four rings is 1.9 λ (as in Fig. 6). The diameter of the elements of the other rings is 2.5 λ. Right panels show the superposition of the array directivity φ-cuts for the boresight (top) and the maximally scanned (bottom) beams.
All the employed circular feeds have been optimally synthesized as shown in [7].

As for the wide beam, the two architectures are equivalent, because they both exploit the layout of Fig. 6. Turning to the narrow beam, the performances of the 424-element layout of Fig. 13 in SLL terms are comparable to those of the 628-element layout of Fig. 10: in both cases the SLL constraint is fully satisfied, even for the maximally scanned beam. Accordingly, to fully satisfy the narrow-beam SLL constraint (even for the maximally scanned beam) the 424-element layout of Fig. 13 employs 33% fewer elements than the 628-element layout of Fig. 10. Moreover, this significant reduction of the number of elements leads to just 0.2 dB of directivity reduction (see Table II). Indeed, the performance index η of the 424-element-layout of Fig. 13 is 1.6 dB higher than that of the 628-element layout of Fig. 10. Summing up, to fully fulfill the zooming/shrinking requirements in (1)-(3) (even for the maximally scanned beam), the first architecture of Fig. 2 requires 628+43=671 elements. Conversely, the second architecture of Fig. 2 requires 424 elements, that is, 37% fewer elements. This overall reduction of the number of control points leads to just to 0.2 dB reduction of the narrow-beam directivity.

We now discuss the comparison between the interleaved-shared zoomable architecture of Fig. 13 and the one obtained in [8].

As remarked above, to fully satisfy the SLL constraints, even for the maximally scanned beams, the sparse layout synthesized in [8] requires 758 elements. Accordingly, with the interleaved-shared architecture of Fig. 13 we have obtained the same SLL performances (for both the wide and the narrow beam) achieved in [8] by exploiting 44% fewer elements. Moreover, this significant reduction of the number of control points has led to an impairment of the directivity of the wide and the narrow beam of just 1.8 dB and 1.1 dB, respectively. In this regard, we stress that, due to the need to radiate with the same layout also the wide beam, in [8] it has been not possible to use a feed dimension larger than 2.2 λ. Conversely, the 424-element layout of Fig. 13 exploits 381 feeds (of 2.5 λ diameter) larger and only 42 feeds (of 1.9 λ diameter) smaller than those used in [8]. Accordingly, the interleaved-shared zoomable architecture of Fig. 13 allows for the radiation of the narrow beam exploiting feeds meanly larger than those used in [8].

Finally, note that the 424-element layout of Fig. 13 satisfies the required steering as well as zooming design specifications with a number of feeds just 15% greater than that of the 368-element layout found in [7] to radiate (still with an isophoric sparse array) only the narrow steerable beam.

TABLE II
RINGS' POSITIONS IN THE OBTAINED ZOOMABLE LAYOUTS

			First architecture (Interleaved layouts)				Second architecture (Interleaved-shared layouts)	
	Wide beam layout (Figure 6)		Narrow beam layout (Figure 9)		Narrow beam layout (Figure 10)		Narrow beam layout (Figure 13)	
1	4	1.34	-	-	-	-	4	1.34
2	10	3.24	-	-	-	-	10	3.24
3	12	5.43	-	-	-	-	12	5.43
4	17	7.82	-	-	-	-	17	7.82
5	-	-	26	10.51	25	10.54	23	11.85
6	-	-	26	13.40	27	13.39	28	14.72
7	-	-	32	16.37	32	16.14	34	17.70
8	-	-	38	19.74	38	19.04	41	20.98
9	-	-	46	23.59	44	22.16	48	24.88
10	-	-	55	28.04	51	25.58	59	30.13
11	-	-	65	33.20	59	29.43	70	35.99
12	-	-	77	39.58	68	33.87	78	39.84
13	-	-	95	48.75	79	39.19	-	-
14	-	-	-	-	93	45.94	-	-
15	-	-	-	-	112	55.55	-	-
Ring index	Number of elements	Radius [λ]	Number of elements	Radius [λ]	Number of elements	Radius [λ]	Number of elements	Radius [λ]

VI. CONCLUSION

In this paper we have addressed the synthesis of isophoric sparse ring arrays for full Earth coverage from GEO satellites through the radiation of steerable as well as zoomable beams.

To this end, starting from an analysis performed on

continuous sources, we have proposed the exploitation of two interleaved sparse arrays deployed over the available circular aperture. In particular, we have presented two slightly different antenna architectures. In one case, the two beams are radiated by two separate interleaved arrays; in the other case, the two beams are, instead, radiated by two interleaved arrays that share a common part of their layouts.

The synthesis of the two architectures has been obtained by means of the cascade of two separate steps, both based on a computationally very efficient deterministic approach. The first step synthesizes the inner sparse array tailored to the wide beam, whereas the second one synthesizes the array tailored to the narrow-beam.

The use of the proposed architectures enabled the required design constraints to be satisfied with a significant reduction of the number of control points compared to non-interleaved sparse architectures. If we look at the same application scenario, with the first architecture proposed in this work we have obtained a 503-element layout with SLL performances comparable to those achieved with the 667-element layout found in [8]. Moreover, with the second architecture proposed in this work we have obtained a 424-element layout with SLL performances comparable to those achieved with the 758-element layout found in [8].

We also fulfilled the required steering as well as zooming design specifications with a number of feeds 37% in the first architecture and just 15% in the second architecture greater than that of the 368-element layout found in [7] to radiate (still with an isophoric sparse array) only the narrow steerable beam.

We finally observe that with both the proposed architectures in order to radiate the wide beam we exploit a number of control points significantly smaller than that devoted to the radiation of the narrow beam. This leads to an imbalance between the powers associated with the two radiated beams, which thus needs to be properly accounted for, by applying, for instance, an increase of the gain of the amplifiers feeding the inner sub-array. It must also be stressed that such a solution can be straightforwardly applied to the first proposed architecture, where the two beams are radiated by two separate arrays. Conversely, application of such a solution to the second architecture requires particular care: it is matter of current study and future work.

AKNOWLEDGEMENT

This work has been supported in part by the European Space Agency under the ESA/ESTEC contract No. 4000102257 *Active Multibeam Sparse Array Demonstrator*.

REFERENCES

[1] Y.Cailloce, G.Caille, I.Albert, J.M.Lopez, "A Ka-band direct radiating array providing multiple beams for a satellite multimedia mission," in *Proc. IEEE 2000 Int. Conf. Phased Array Syst. Technol.*, May 2006, pp. 403 – 406,

[2] G.Toso, C.Mangenot, and A.G.Roederer, "Sparse and thinned arrays for multiple beam satellite applications," in *Proc. 29th ESA Antenna Workshop Multiple Beams Reconf. Antennas*, Apr. 2007, pp. 207–210.

[3] ESA/ESTEC Tender AO/1-5598/08/NL/ST. (2008). *Innovative Architectures For Reducing The Number Of Controls Of Multiple Beam Telecommunications Antennas* [Online]. Available: www.esa.int.

[4] ESA/ESTEC Tender AO/1-6338/09/NL/JD. (2009) *Active Multibeam Sparse Array Demonstrator* [Online]. Available: www.esa.int.

[5] M.C.Viganò *et al.* "Sparse antenna array for Earth-coverage satellite applications," in *Proc. 4th Eur. Conf. Antennas Propagat.* (EUCAP 10), Barcelona, Spain, 2010, pp.1-4.

[6] G.Toso and R. Mailloux, "Guest editorial for the special issue on innovative phased array antennas based on non-regular lattices and overlapped subarrays," *IEEE Trans. Antennas Propagat.*, vol. 62, no. 4, pp. 1546-1548, Apr. 2014.

[7] O.M.Bucci, T.Isernia, S.Perna, D.Pinchera, "Isophoric sparse arrays ensuring global coverage in satellite communications," *IEEE Trans. Antennas Propagat.*, vol. 62, no. 4, pp. 1607-1618, Apr. 2014.

[8] O.M.Bucci, S.Perna, D.Pinchera; "Synthesis of isophoric sparse arrays allowing zoomable beams and arbitrary coverage in satellite communications," *IEEE Trans. Antennas Propagat.*, vol. 63, Issue 5, pp. 1445 - 1457, Apr. 2015.

[9] M.I.Skolnik, "Nonuniform arrays" in *Antenna Theory*, R. E. Collin and F.Zucker, Eds, New York, NY, USA: McGraw-Hill, 1969, ch. 6, Part I.

[10] M. Vicente-Lozano, F. Ares-Pena, E. Moreno, "Pencil-beam pattern synthesis with a uniformly excited multi-ring planar antenna," *IEEE Antennas Propag. Mag.*, vol. 42, no. 6, pp. 70-74, Dic. 2000.

[11] T.M.Milligan, "Space-tapered circular (ring) array," *IEEE Antennas Propag. Mag.*, vol. 46, no. 3, pp. 70-73, Jun. 2004.

[12] M.C. Viganó, G. Toso, G. Caille, C. Mangenot, I.E. Lager, "Sunflower array antenna with adjustable density taper," *Int. J. Antennas Propagation (Hindawi Publishing)*, pp. 1-10, 2009

[13] D. Caratelli, M.C. Viganò, "A novel deterministic synthesis technique for constrained sparse array design problems," *IEEE Trans. Antennas Propagat*, vol. 59, no. 11, pp. 4085 - 4093, Nov. 2011.

[14] D. Caratelli, M.C. Viganò, "Analytical synthesis technique for linear uniform-amplitude sparse arrays," *Radio Science*, vol. 46, no. 4, Jul. 2011.

[15] P. Angeletti, G. Toso, "Synthesis of circular and elliptical sparse arrays," *Elect. Lett.*, vol. 47, no. 5, pp. 304-306, Mar. 2011.

[16] O. M. Bucci, S. Perna, "A deterministic two dimensional density taper approach for fast design of uniform amplitude pencil beams arrays," *IEEE Trans. Antennas Propagat.*, vol. 59, no. 8, pp. 2952-2861, Aug 2011.

[17] O.M.Bucci, S. Perna, D. Pinchera, "Advances in the deterministic synthesis of uniform amplitude pencil beam concentric ring arrays," *IEEE Trans. Antennas Propagat.*, vol. 60, no. 7, pp. 3504-3509, Jul. 2012.

[18] O. M. Bucci, D. Pinchera, "A generalized hybrid approach for the synthesis of uniform amplitude pencil beam ring-arrays," *IEEE Trans. Antennas Propagat.*, vol. 60, no.1, pp. 174-183, Jan. 2012.

[19] F.Viani, G. Oliveri, A. Massa, "Compressive sensing pattern matching techniques for synthesizing planar sparse arrays," *IEEE Trans. Antennas Propagat.*, vol. 61, no. 9, pp. 4577-4587, Sep.2013.

[20] P. Angeletti, G. Toso, G. Ruggerini, "Array antennas with jointly optimized elements positions and dimensions part ii: planar circular arrays," *IEEE Trans. Antennas Propagat.*, vol. 62, n. 4, Part 1, pp. 1627-1639, Apr. 2014.

[21] M. Carlin, G. Oliveri, A. Massa, "Hybrid BCS-deterministic approach for sparse concentric ring isophoric arrays," *IEEE Trans. Antennas Propagat.*, vol. 63, no. 1, pp. 378-383, Jan. 2015.

[22] O. M. Bucci, T. Isernia, A. Morabito, "An effective deterministic procedure for the synthesis of shaped beams by means of uniform-amplitude linear sparse arrays," *IEEE Trans. Antennas Propagat.*, vol. 61, no. 1, pp. 169-175, Jan. 2013.

[23] O. M. Bucci, T. Isernia, and A. F. Morabito, "Optimal synthesis of directivity constrained pencil beams by means of circularly symmetric aperture fields," *IEEE Antennas Wireless Propag. Lett.*, vol. 8, pp. 1386-1389, Dec. 2009.

[24] O. M. Bucci, T. Isernia, A. F. Morabito, S. Perna, D. Pinchera; "Density and element-size tapering for the design of arrays with a reduced number of control points and high efficiency," in *Proc. 4th Eur. Conf. Antennas Propagat.* (EUCAP 10), Barcelona, Spain, 2010, pp.1-4.